Minimizing Energy Consumption of Wheeled Mobile Robots via Optimal Motion Planning

Shuang Liu and Dong Sun, *Senior Member, IEEE*

***Abstract*—This paper presents a new optimal motion planning aiming to minimize the energy consumption of a wheeled mobile robot in robot applications. A model that can be used to formulate the energy consumption for kinetic energy transformation and for overcoming traction resistance is developed first. This model will provide a base for minimizing the robot energy consumption through a proper motion planning. To design the robot path, the A* algorithm is employed to generate an energy-efficient path where a new energy-related criterion is utilized in the cost function. To achieve a smooth trajectory along the generated path, the appropriate arrival time and velocity at the defined waypoints are selected for minimum energy consumption. Simulations and experiments are performed to demonstrate the energy-saving efficiency of the proposed motion planning approach.**

***Index Terms*—Minimum energy consumption, mobile robot, motion planning.**

I. Introduction

INCREASING energy costs have placed extreme pressure on designers to develop energy-efficient systems and on users to utilize such systems. Despite various energy conservation techniques in different industries, the issue of energy minimization in the robotics field has not been sufficiently studied. In this paper, a new optimal motion planning approach is proposed, aiming to minimize the energy consumption of a wheeled mobile robot in robot applications.

Energy consumption of mobile robots can be minimized by improving the energy efficiency of a robot system, including its motors and motor drivers. Optimization of robot applications can also contribute to energy conservation [1]. Motion planning has recently emerged as a way to minimize energy consumption during robot motion. Minimum energy velocity planning was proposed in [2], which could save battery energy by up to 10% compared with the widely used trapezoidal velocity profile. Energy-efficient motion planning for robot exploration was proposed in [3], which could save up to 42% energy compared with the common utility-based method.

To improve productivity efficiency, numerous energy-efficient motion planning approaches have been applied to industrial robots [4], [5]. Energy-efficient motion planning was also used for other types of robots such as a space manipulator [6], humanoid robot [7], rover robot [8], soccer robot [9], and biorobot for cell manipulation [10]. Energy-efficient motion planning for mobile robots has recently attracted considerable attention [11]–[13] to meet requirements for mobile robots in various applications. Deployment of mobile robots with energy constraints was addressed in [14]. Effective path planning was designed to enable a robot to accomplish a series of tasks by using minimum energy in [15]. In [16], energy constraints were considered in studying the issue of multiple sensor coverage.

Various criteria have been applied in the design of objective functions to save energy. A number of researchers incorporated the criteria of the shortest path length into the objective function to minimize energy consumption [17]. The loss of kinetic energy was used to test robot motion performance in saving energy in [18]. Minimum energy was achieved by reducing the steering actuations of robots in optimal trajectory planning in [19]. Trajectory smoothness was also used as a criterion in the objective function of trajectory planning and is based on an assumption that the robot requires less energy when moving along a smoother trajectory [20]. In all studies aforementioned, a model that can be used to formulate the energy consumption of a mobile robot was not fully investigated. Establishing such a model provides a solid foundation for energy minimization efforts.

In this paper, an energy model is established for wheeled mobile robots, and based on which an optimal motion planning is developed to minimize energy consumption in robot applications. The main contributions of this paper are twofold.

First, the energy consumption model developed for a two-wheeled mobile robot has been successfully used for motion planning aiming for minimizing the robot energy consumption. The matters, including resources that consume energy such as motors, sensors, and onboard computers, the influence caused by ground friction and the workload of robots, are considered in the modeling. In existing works, the energy model was assumed to be a polynomial function of robot velocity in [21], and motor resistances were considered the main source of energy dissipation in wheeled robots in [2]. In our proposed study, the energy consumption is analyzed from three aspects: kinetic energy transformation, overcoming traction resistance, and maintenance of electric sources for the operation of sensors, onboard PCs, and control circuits, etc. Experiments indicate that the developed energy model can determine the actual energy consumption.

Second, based on the proposed energy model, a novel optimal motion planning is proposed to minimize the energy consumption during the robot motions. In path planning, the A*-based

Manuscript received March 6, 2012; revised July 27, 2012 and November 20, 2012; accepted January 14, 2013. Date of publication February 8, 2013; date of current version February 20, 2014. Recommended by Technical Editor M. Iwasaki. This work was supported in part by the Research Grants Council, Hong Kong Special Administrative Region, China, under Grant CityU 120709.

The authors are with the Department of Mechanical and Biomedical Engineering, City University of Hong Kong, Kowloon, Hong Kong (e-mail: shuangliu2@cityu.edu.hk; medsun@cityu.edu.hk).

Color versions of one or more of the figures in this paper are available online at http://ieeexplore.ieee.org.

Digital Object Identifier 10.1109/TMECH.2013.2241777

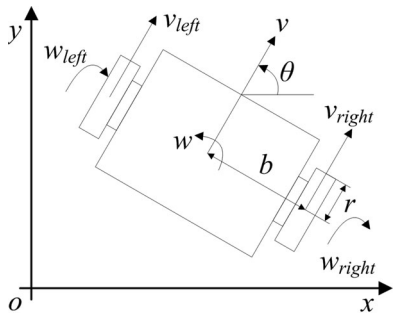

Fig. 1. Structure of a two-wheeled mobile robot.

path planner [22] has been used to design a collision-free path. This path planner can identify the least cost path from a given initial node to the goal node, e.g., the shortest path for energy saving [17]. Unlike the traditional A* planner, in this paper, a new energy-related criterion in relation to important factors such as the load on the robot, the ground friction, and environmental conditions, etc., is added to the cost function of the A* algorithm. To smooth the trajectory along the generated path, the trajectory is further optimized by selecting the arrival time and velocity at each waypoint, with a new objective function that considers energy consumption based on the established energy model. Experiments demonstrate that the proposed motion planning approach that treats energy saving as the central criteria can better minimize energy consumption than the approach with other criterion such as kinetic energy loss [18], steering actuations [19], and trajectory smoothness [20].

The remainder of this paper is organized as follows. In Section II, the energy model of a two-wheeled mobile robot is developed. In Section III, A* path planner with the new energy criteria is developed to generate a collision-free path. By utilizing waypoints of the generated path, a parameterized trajectory is smoothed with an appropriate arrival time and velocity at each waypoint in Section IV. In Section V, the modeling parameters are identified in an example that uses the Pioneer 3DX mobile robot. Simulations and experiments are performed to demonstrate the effectiveness of the proposed motion planning approach to minimizing energy consumption. Section VI concludes this work.

II. Energy Model of a Two-Wheeled Mobile Robot

In a mobile robot with common architecture, energy is consumed primarily by the functions of its motors, sensors, microcontroller, and embedded computer [4], [21]. In this section, an energy consumption model for a two-wheeled mobile robot is developed.

Fig. 1 illustrates the structure of a two-wheeled mobile robot that is characterized by a symmetrical structure and is driven by two identical DC motors. $q = [x, y, \theta]^T$ is denoted as the robot coordinates, where x and y denote the linear coordinates, and θ is the orientation. Robot kinematics can be represented by

$$\dot{q} = \begin{bmatrix} \dot{x} \\ \dot{y} \\ \dot{\theta} \end{bmatrix} = \begin{bmatrix} \cos\theta \\ \sin\theta \\ 0 \end{bmatrix} v + \begin{bmatrix} 0 \\ 0 \\ 1 \end{bmatrix} w \tag{1}$$

where v and w denote the linear and angular velocities with respect to the center of mass of the robot, respectively. Note that no slippage is considered between the robot wheels and ground.

Denote w_{left} and w_{right} as the angular velocity of the left and the right wheels, respectively, expressed by

$$\begin{bmatrix} w_{\text{left}} \\ w_{\text{right}} \end{bmatrix} = \frac{1}{r} \begin{bmatrix} 1 & -b \\ 1 & b \end{bmatrix} \begin{bmatrix} v \\ w \end{bmatrix} \tag{2}$$

where r denotes the radius of the wheel, and b denotes the distance between the center of the robot and the two wheels, as shown in Fig. 1.

Among the main sources of energy consumption of a wheeled mobile robot are the motors and other components such as onboard computers, sensors, and electric circuits. In the following section, a detailed analysis will be given from two perspectives.

The energy consumed for motors include two main parts: the energy transformed into robot kinetic energy and the energy to overcome traction resistance. In this study, transforming loss is neglected as in [14].

The kinetic energy of the robot can be expressed as

$$\begin{aligned} E_{\text{kinetic}} &= \frac{1}{2} m v(t)^2 + \frac{1}{2} I w(t)^2 \\ &= \int_t \left(d\left(\frac{1}{2} m v(t)^2\right) + d\left(\frac{1}{2} I w(t)^2\right)\right) \\ &= \int_t \left(m v(t) a(t) + I w(t) \beta(t)\right) dt \end{aligned} \tag{3}$$

where m and I denote the mass and the moment of inertia of the robot, respectively; while a and β denote the linear and angular accelerations, respectively. Given that the moment of inertia of the wheels is relatively small, the rotational energy of the robot wheels is not considered in (3).

For most motors, the kinetic energy cannot be well transformed back to the electric energy. The energy is lost mainly due to heat loss during the deceleration, when $v(t)a(t) < 0$ or $w(t)\beta(t) < 0$. Therefore, the consumed energy that is used to increase the robot kinetic energy is expressed as

$$E_{\text{kinetic}} = \int_t \left(m \max\{v(t)a(t), 0\} + I \max\{w(t)\beta(t), 0\}\right) dt \tag{4}$$

where the function max{} yields the maximum value in the brackets.

During robot motion, the motors provide energy to overcome traction resistance that is mainly from rolling friction of the two wheels. This energy loss depends on the weight and the payload of the robot and the ground types. Note that there is no slippage between wheels and ground, and hence, dynamic friction is not considered [23].

The power drawn by the terrain from the two wheels, denoted by P_{left} and P_{right}, can be modeled by

$$\begin{bmatrix} P_{\text{left}} \\ P_{\text{right}} \end{bmatrix} = \mu\, mg \begin{bmatrix} |v_{\text{left}}| \\ |v_{\text{right}}| \end{bmatrix} \tag{5}$$

where g denotes gravitational acceleration, and *mg* denotes all the weight and payload of the robot. μ is the rolling friction coefficient that depends on the surface type of the ground. v_{left}

and v_{right} denote the velocity of the left and right wheels, respectively. Based on Fig. 1, the velocities of the two wheels are described as

$$\begin{bmatrix} v_{\text{left}} \\ v_{\text{right}} \end{bmatrix} = \begin{bmatrix} 1 & -b \\ 1 & b \end{bmatrix} \begin{bmatrix} v \\ w \end{bmatrix}. \tag{6}$$

Substituting (6) into (5) yields

$$\begin{bmatrix} P_{\text{left}} \\ P_{\text{right}} \end{bmatrix} = \mu mg \begin{bmatrix} |v(t) - bw(t)| \\ |v(t) + bw(t)| \end{bmatrix}. \tag{7}$$

Energy consumption attributed to traction resistance can then be derived as follows:

$$E_{\text{res}}(t) = \int_t (P_{\text{left}} + P_{\text{right}})\, dt. \tag{8}$$

Substituting (7) into (8) yields

$$\begin{aligned} E_{\text{res}}(t) &= \int_t \mu mg \left(|v(t) - bw(t)| + |v(t) + bw(t)|\right) dt \\ &= \begin{cases} 2\mu mg \int_t |v(t)|\, dt & |v(t)| \geq |bw(t)| \\ 2\mu mg \int_t b\,|w(t)|\, dt & |v(t)| < |bw(t)| \end{cases} \\ &= 2\mu mg \int_t \max\left\{|v(t)|, b\,|w(t)|\right\} dt \end{aligned} \tag{9}$$

where the term $\max\{|v(t)|, |bw(t)|\}$ yields the maximum of $|v(t)|$ and $|bw(t)|$. Note that $\int_t |v(t)|\, dt$ approximately equals the travel length s.

By combining (4) and (9), the energy consumption attributed to motors during robot motion is obtained as

$$\begin{aligned} E_{\text{motor}}(t) &= E_{\text{kinetic}} + E_{\text{res}} \\ &= \int_t \begin{pmatrix} m \max\{v(t)a(t), 0\} + I \max\{w(t)\beta(t), 0\} \\ + 2\mu mg \max\{|v(t)|, |bw(t)|\} \end{pmatrix} dt. \end{aligned} \tag{10}$$

The energy consumed by the onboard computer, sensors, and electric circuit is then considered. Energy consumption of these nonmechanical components within a unit of time is relatively stable and can be presented as the power consumption P_s. Total energy consumption then becomes $E_{\text{other}}(t) = P_s t$.

Finally, the energy model of a two-wheeled mobile robot in terms of energy consumption for the motor and for other components is expressed as

$$\begin{aligned} E_{\text{total}} &= E_{\text{motor}} + E_{\text{other}} \\ &= \int_t \begin{pmatrix} m \max\{v(t)a(t), 0\} + I \max\{w(t)\beta(t), 0\} \\ + 2\mu mg \max\{|v(t)|, |bw(t)|\} \end{pmatrix} dt + P_s t. \end{aligned} \tag{11}$$

By employing the aforementioned energy model, a motion planning method for the minimization of robot energy consumption is developed in the subsequent sections.

III. Optimal Path With Minimum Energy Cost

In this section, an A* algorithm is used with a new energy-related criterion to identify a collision-free path. This algorithm considers obstacle avoidance and minimum energy consumption.

A. A* Algorithm

The A* algorithm has been widely used in path generation [22]. Based on the defined cost criterion, A* uses a best first search and then identifies a least cost path from a given initial node to the goal node. By utilizing this property, a new cost function with the energy-saving criterion is proposed in this paper to search for an optimal path with minimum energy.

A grid map is used to present the cluttered environment, in which the distribution of obstacles can be shown [22]. Each grid is considered to be a node that is either free or occupied by obstacles. k is defined as the index of node. By using the A* algorithm, the search is initiated in the start node, and the cost of the path from the start node to the node k, which is denoted by $g_a(k)$, can be calculated based on the travel distance [22]

$$g_a(k) = g_a(k-1) + s_k \tag{12}$$

where s_k denotes the travel distance between the two nodes $k-1$ and k. A least cost path is then identified according to the path costs of the nodes [22].

The order of the path-cost calculation of different nodes is important. In the A* algorithm, this order is determined by the cost function $f_a(k)$, which includes the cost $g_a(k)$ and a "heuristic estimate" of the cost of the path from the node k to the goal, described as follows:

$$f_a(k) = g_a(k) + h_a(k) \tag{13}$$

where $h_a(k)$ denotes the heuristic function. The node with the least cost of $f_a(k)$ is always checked first in the search. In this sense, the A* algorithm is a best first search algorithm characterized by high searching efficiency. By using the heuristic function, the least cost path can be found without calculating the path costs of all the nodes in the grid map. If the heuristic function is not used, $h_a(k)$=0, A* algorithm will then degenerate to a breadth-first search algorithm.

However, the shortest path may not necessarily result in minimum energy consumption because other factors (e.g., ground conditions) also have a significant effect on energy consumption. In the following section, a new energy-related criterion will be used in the cost function of the path planner for minimizing energy consumption. Given that the same framework of the A* planner is used, the main property of the A* algorithm is preserved in the proposed path planner.

Remark: Setting the grid resolution is important when the A*-based path planning is used. The use of coarser grids results in a faster path-searching process. However, the paths that pass through narrow portions may not be easily found. Furthermore, the number of points on the grid grows exponentially in the configuration space dimension. In this paper, the grid resolution is set based on the size of robots and the obstacles. The experiments indicate that efficient searching performance can be achieved when the grid size is set to approximately half of the robot size.

B. Path Planning With Minimum Energy Consumption

As seen in the energy model (12), energy consumption is closely related to the load of the robot and to the ground condition, which will be considered in the following A*-based path planner. Given that robot velocity is unknown in path planning, robot motion is not considered in path planning but is considered in trajectory smoothing in Section IV.

The load of the robot affects the friction and is considered first. p_k is denoted as the node; and $p_{k-1}p_k$ is the path segment between nodes p_{k-1} and p_k, where $k = 1, 2, \ldots, L$ is the index of node, and L is the total number of nodes. p_0 denotes the start point. A new energy-related criterion is proposed as

$$\begin{aligned} g_a(k) &= g_a(k-1) + 2\mu_{k-1,k}\, mg \int_t |v(t)|\, dt \\ &= g_a(k-1) + 2\mu_{k-1,k}\, mg\, s_{k-1,k} \end{aligned} \tag{14}$$

where $\mu_{k-1,k}$ is the friction parameter, and $s_{k-1,k}$ denotes the length of the path segment $p_{k-1}p_k$. The second term on the right-hand side of (14) represents energy consumption attributed to the rolling friction of the robot wheels along the path segment, based on (9).

The ground condition is further considered. For safety, the generated path should maintain a large distance from obstacles. If a node is close to surrounding obstacles, it should not be chosen by the generated path. Thus, a penalty factor, denoted by $\rho_{\text{obs}}(k) \in [0, 1]$, is incorporated into the criterion (14)

$$g_a(k) = g_a(k-1) + 2\mu_{k-1,k}, mg\, s_{k-1,k} \frac{1}{\rho_{\text{obs}}(k)} \tag{15}$$

where $\rho_{\text{obs}}(k)$ for the node p_k is defined as

$$\rho_{\text{obs}}(k) = \begin{cases} 1, & d_{\text{obs}} > D_{\text{safe}} \\ \dfrac{d_{\text{obs}} - b}{D_{\text{safe}} - b}, & b < d_{\text{obs}} \le D_{\text{safe}} \\ 0, & d_{\text{obs}} \le b \end{cases} \tag{16}$$

where d_{obs} is the minimum distance between the concerned node and the nearest obstacle, and D_{safe} is a safety distance that is large enough for a safe motion.

If $d_{\text{obs}} > D_{\text{safe}}$ and $\rho_{\text{obs}}(k) = 1$, the node is far away from obstacles, and the inclusion of the penalty factor does not change the criteria (15). If $d_{\text{obs}} \le b$ and $\rho_{\text{obs}}(k) = 0$, the node is too close to the obstacle, and the path cost becomes infinitely large. If $b < d_{\text{obs}} \le D_{\text{safe}}$, the path cost increases as the distance d_{obs} decreases.

The heuristic function $h_a(k)$ estimates the cost from the node p_k to the destination p_L in the A* algorithm. The heuristic function is defined such that the estimated path cost is not higher than the actual cost from the node to the goal. If this condition is not fulfilled, the path cannot be found [22].

Define the heuristic function as

$$h_a(k) = 2\mu_{k-1,k}\, mg\, s_{k,L} \tag{17}$$

where $s_{k,L}$ denotes the distance between p_k and p_L. The penalty factor is not considered here.

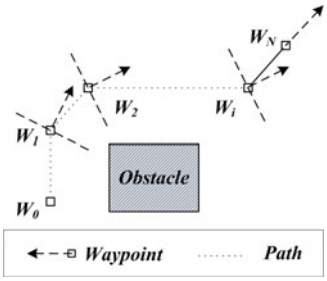

Fig. 2. Selection of waypoints.

Finally, the new cost function can be obtained by substituting (16) and (17) into (13)

$$f_a(k) = g_a(k-1) + 2\mu_{k-1,k}\, mg \left(\frac{s_{k-1,k}}{\rho_{\text{obs}}(k)} + s_{k,L} \right). \tag{18}$$

By using the cost function (18), an optimal collision-free path with minimum energy consumption can be obtained.

IV. Parameterized Trajectory With Minimum Energy Consumption

This section presents trajectory smoothing based on the generated path while minimizing energy consumption through parameter optimization.

A. Waypoint Selection and Trajectory Planning

For the advantages of continuity and controllability [24], a cubic Bézier curve is used to smooth the trajectory path. The smooth trajectory between the start and goal postures is a combination of a series of connected cubic Bézier curves. A series of waypoints from the start to the goal are defined, with the information of their positions and orientations for generating cubic Bézier curves.

Based on the generated geometric path described previously, the waypoints can be defined as follows. The start and goal positions as well as the knee points along the path are selected as waypoints. Two neighboring waypoints are combined if they are sufficiently close, and new waypoints may be inserted if a path segment is extremely long [25]. In this way, a series of waypoints, denoted by $W_0, W_1, \ldots, W_i, \ldots, W_N$, can be obtained. The orientations of these waypoints can be defined in the following way. The orientation of the start waypoint W_0 is the same as the initial robot orientation θ_0, and the tangent orientation of the final waypoint W_N is the same as the robot orientation at the end position or along the direction of the last line segment. The orientations of the other waypoints are set perpendicular to the angular bisector of the two neighboring line segments, in a similar manner as that in the common heuristic method [26], as shown in Fig. 2.

Trajectory planning aims to generate a smooth function of the robot state with respect to time. The generated trajectory connects two neighboring waypoints W_{i-1} and W_i $(i = 1, \ldots, N)$ such that the robot can approach the final goal W_N along all these waypoints. The positions and orientations of W_{i-1}

and W_i are denoted as $q_{i-1} = [X_{i-1}, Y_{i-1}, \theta_{i-1}]^T$ and $q_i = [X_i, Y_i, \theta_i]^T$, respectively. By using the parameterized cubic Bézier curve to achieve curve continuity, the trajectory is represented as follows [23]:

$$\begin{cases} x(u_i) = (1-u_i)^3 X_{i-1} + 3u_i(1-u_i)^2 X_{ai} \\ \qquad + 3u_i^2(1-u_i)X_{bi} + u_i^3 X_i \\ y(u_i) = (1-u_i)^3 Y_{i-1} + 3u_i(1-u_i)^2 Y_{ai} \\ \qquad + 3u_i^2(1-u_i)Y_{bi} + u_i^3 Y_i \end{cases} \tag{19}$$

where $x(u_i)$ and $y(u_i)$ ($u_i \in [0,1]$) are functions of the trajectory in the x- and y-direction, respectively; and (X_{ai}, Y_{ai}) and (X_{bi}, Y_{bi}) are the parameters to be designed.

When u_i varies from 0 to 1, $(x(u_i), y(u_i))$ varies continuously from (X_{i-1}, Y_{i-1}) to (X_i, Y_i). For each segment $W_{i-1}W_i$, the end waypoint W_i is also the start point of the next segment W_iW_{i+1}. Therefore, $u_i = \frac{t-T_{i-1}}{T_i - T_{i-1}}$ is introduced as an intermediate variable for $t \in [T_{i-1,i}, T_i]$, where $T_i (i = 1, \ldots, N)$ denotes the arrival time at each waypoint from the beginning ($T_0 = 0$). In this manner, when t varies from T_0 to T_N, $(x(t), y(t))$ varies from W_0 to W_N.

Define V_{i-1} and V_i as the velocities at waypoints W_{i-1} and W_i, respectively. The trajectory can be identified based on the cubic Bézier curve and is subject to the following kinematics constraints:

$$\begin{aligned} \left.\frac{dx(u_i)}{dt}\right|_{t=T_{i-1}} &= \frac{3(X_{ai} - X_{i-1})}{T_i - T_{i-1}} = V_{i-1}\cos\theta_{i-1} \\ \left.\frac{dy(u_i)}{dt}\right|_{t=T_{i-1}} &= \frac{3(Y_{ai} - Y_{i-1})}{T_i - T_{i-1}} = V_{i-1}\sin\theta_i \\ \left.\frac{dx(u_i)}{dt}\right|_{t=T_i} &= \frac{3(X_i - X_{bi})}{T_i - T_{i-1}} = V_i\cos\theta_i \\ \left.\frac{dy(u_i)}{dt}\right|_{t=T_i} &= \frac{3(Y_i - Y_{bi})}{T_i - T_{i-1}} = V_i\sin\theta_i. \end{aligned} \tag{20}$$

Parameters X_{ai}, Y_{ai}, X_{bi}, and Y_{bi} are dependent on the arrival time T_i and on the velocity V_i. These parameters can be derived from (20) as follows:

$$\begin{aligned} X_{ai} &= X_{i-1} + \frac{1}{3}(T_i - T_{i-1})V_{i-1}\cos\theta_{i-1} \\ Y_{ai} &= Y_{i-1} + \frac{1}{3}(T_i - T_{i-1})V_{i-1}\sin\theta_{i-1} \\ X_{bi} &= X_i - \frac{1}{3}(T_i - T_{i-1})V_i\cos\theta_i \\ Y_{bi} &= Y_i - \frac{1}{3}(T_i - T_{i-1})V_i\sin\theta_i. \end{aligned} \tag{21}$$

Therefore, by selecting an appropriate T_i and V_i, an optimized trajectory can be obtained.

B. Parameter Optimization for Energy Minimization

In this section, parameters T_i and V_i are selected to minimize energy consumption. The energy consumption of the robot along the trajectory from W_0 and W_N based on the energy model (11) is expressed as

$$\begin{aligned} E_{0,N} &= P_s T_N \\ &+ \int_0^{T_N} \begin{pmatrix} m\max\{v(u_i)a(u_i), 0\} + I\max\{w(u_i)\beta(u_i), 0\} \\ + 2\mu g\max\{|v(u_i)|, |bw(u_i)|\} \end{pmatrix} dt \end{aligned} \tag{22}$$

where $v(u_i)$ and $w(u_i)$ denote the linear and angular velocities along the trajectory within the segment W_iW_{i+1}, respectively; and $a(u_i)$ and $\beta(u_i)$ denote the linear and angular accelerations, respectively.

By utilizing the parameterized trajectory (19), the linear velocity $v(u_i)$ can be derived as

$$v(u_i) = \left(\left(\left.\frac{dx(u_i)}{du_i}\right|_t \right)^2 + \left(\left.\frac{dy(u_i)}{du_i}\right|_t \right)^2 \right)^{\frac{1}{2}}. \tag{23}$$

Notably, $v(u_i)$ is a function of the parameters (X_{ai}, Y_{ai}) and (X_{bi}, Y_{bi}) and can be obtained by substituting (19) into (23). Given that parameters X_{ai}, Y_{ai}, X_{bi}, and Y_{bi} depend on T_i and V_i, the robot velocity $v(u_i)$ also depends on T_i and V_i.

The angular velocity $w(u_i)$ can be calculated by using the curvature of the curve $\delta(u_i)$, i.e., $w(u_i) = \delta(u_i)v(u_i)$, where

$$\delta(u_i) = \frac{\frac{d^2y(u_i)}{du_i^2}\frac{dx(u_i)}{du_i} - \frac{d^2x(u_i)}{du_i^2}\frac{dy(u_i)}{du_i}}{\left(\left(\frac{dx(u_i)}{du_i}\right)^2 + \left(\frac{dy(u_i)}{du_i}\right)^2\right)^{\frac{3}{2}}}. \tag{24}$$

The acceleration $a(u_i)$ and $\beta(u_i)$ can be calculated by differentiating the linear and angular velocities, which also depend on T_i and V_i.

As the values of $v(u_i), w(u_i), a(u_i)$, and $\beta(u_i)$ all depend on T_i and V_i as described previously, the energy consumption (22) can be optimized by selecting an appropriate arrival time T_i and velocity V_i at each segment W_iW_{i+1}. The minimum energy consumption can thus be obtained through the use of an iterative algorithm for choosing the parameters T_i and V_i. The pseudocodes are given as follows.

Given T_i and $V_i, i = 1, \ldots, N$, calculate $E_{0,N}$ in the following way.

//In each segment W_iW_{i+1}, calculate the following variables sequentially:

calculate: X_{ai}, Y_{ai}, X_{bi}, and Y_{bi} based on (21);
calculate: $x(u_i)$ and $y(u_i)$ based on (19);
calculate: $v(u_i)$ based on (23);
calculate: $w(u_i), \delta(u_i)$based on (24);
calculate: $E_{i,i+1}$ based on (22);
calculate: $E_{0,N}$; //sum all $E_{i,i+1}, i = 1, \ldots, N$.
Select T_i and V_i that yield the minimum value of $E_{0,N}$.

V. Simulations and Experiments

A. Experimental Identification of Energy Model for Pioneer 3DX Mobile Robot

The proposed energy model can be used for any two-wheeled mobile robot with kinematics (1). For different robots, the modeling parameters μ and P_s differ and must first be identified

TABLE I
PIONEER 3DX PARAMETERS

Robot parameters		Values
r	wheel radius	9.25 (cm)
b	robot radius	18.5 (cm)
m	mass	9 (kg)
I	moment of inertia	0.16245 (kg m^2)

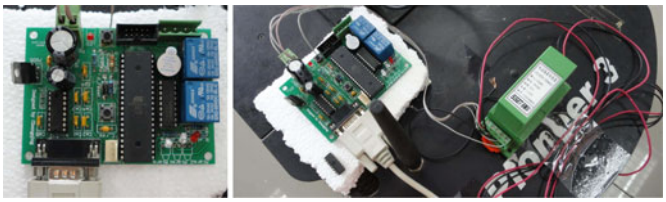

Fig. 3. Current sensing hardware. (Left) Data acquisition. (Right) Current sensor.

before applying the energy model. In the following section, the two-wheeled Pioneer 3DX robot is used as a reference platform [27], and the parameters μ and P_s are then identified.

The Pioneer 3DX robot weighs approximately 9 kg and can carry a load that weighs a maximum of 23 kg. The robot features an onboard computer and accessories and is equipped with sonar arrays for sensing and wireless communication. The robot is driven by two Pittman DC motors that are controlled by a Hitachi H8 S-based microcontroller. The detailed parameters of the robot are listed in Table I.

A current sensing system that performs data acquisition was developed to monitor the current that travels to the motor and that drawn from the batteries, as shown in Fig. 3. The measured current was sampled via data acquisition with 20 kHz sampling rate. The voltage used was 12 V. The consumed power was measured as a product of the voltage and the measured current.

Experimental tests were performed to identify the parameters μ and P_s in the energy model (11) for the Pioneer 3DX robot. The parameter μ was identified by driving the robot in a straight line on a marble surface. In the experiment, the robot accelerated from zero to the desired velocity within 2.5 s. The robot maintained this velocity for 5 s and then decreased its velocity to zero with a deceleration time of 2.5 s. The desired velocity ranged from 0.05 m/s to 0.7 mm/s with a step of 0.05 mm/s. The input currents to the motors were measured and collected, as shown in Fig. 4. To illustrate the results more clearly, only currents with velocities of 0.05, 0.2, 0.4, 0.6, and 0.7 m/s are shown in Fig. 4.

The current increased as the motor speed increased. The current became relatively stable during constant motion and then reduced when the motors decelerated. These results agreed with the energy consumption model for motors, as specified in (10). When the robot was still, a fixed current of approximately 13.6 mA was transferred to the motors to provide energy to maintain the basic function of the control circuit. This current should be considered, especially when identifying the parameter P_s.

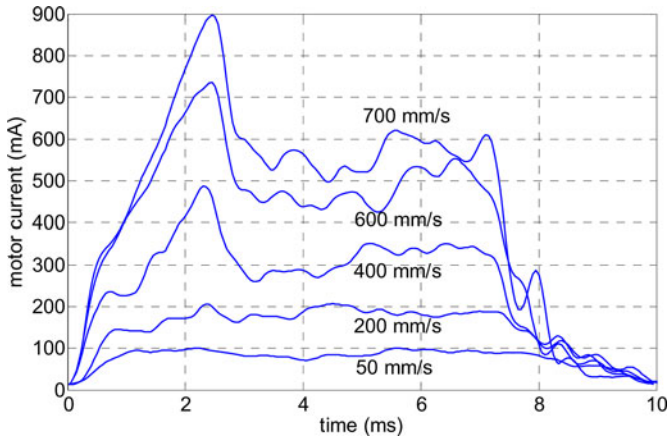

Fig. 4. Motor's input current with respect to velocity.

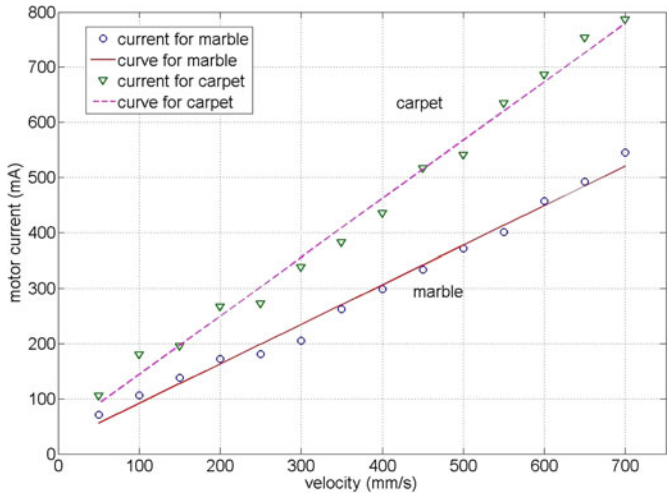

Fig. 5. Motor current versus robot velocity.

When the robot moved at a constant speed in the experiments, the energy consumption by the motors in (10) was simplified as

$$E_{\text{motor}}(t) = 2\mu mg\, vt. \tag{25}$$

The parameter μ varies for different ground surfaces. To understand this issue, the robot was driven on two different floor surfaces: marble and carpet. The experimental results are shown in Fig. 5. The relationship between the motor's current and the robot velocity v could be obtained by fitting the curve by using the MATLAB tool "cftool" (see Fig. 5). The parameter μ was then estimated based on (25). For the marble surface, $\mu \approx 0.051 \pm 0.005$; and for the carpet surface, $\mu \approx 0.082 \pm 0.005$.

The parameter P_s was then identified by letting the robot stop at a fixed position while turning the power on to monitor the current drawn from the batteries. In this situation, the energy consumption for motors was zero, and only the energy consumption for the other components was counted. The battery current was stable, and the parameter P_s was calibrated at (17.7 ± 0.5) W.

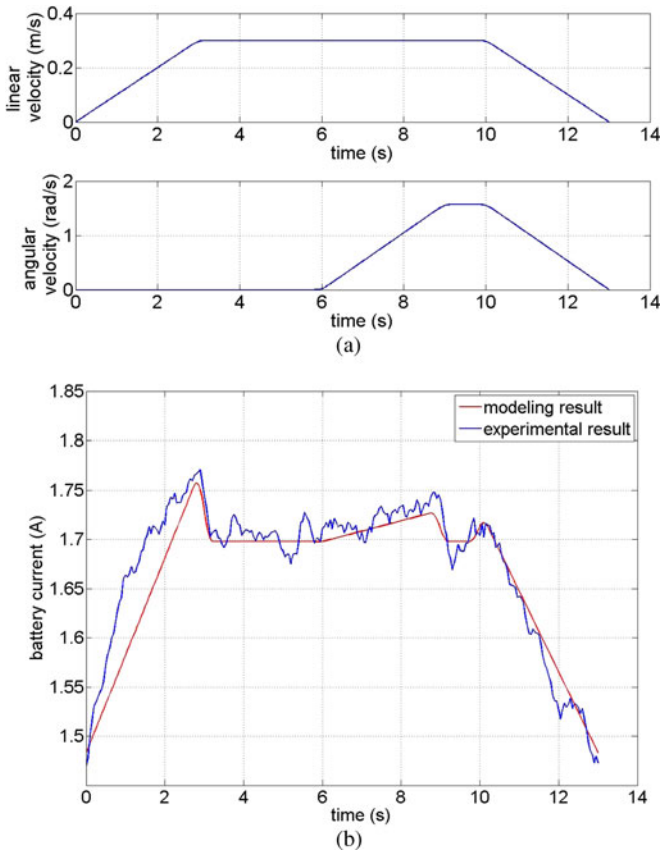

Fig. 6. Model verification experiment. (a) Velocity profile. (b) Comparison between modeling and experimental results.

Finally, the energy model of the two-wheeled Pioneer 3DX mobile robot on the marble floor was calibrated as

$$E_{\text{total}}(t) = 17.7t + \int_t \begin{pmatrix} 9v(t)a(t) + 0.16245w(t)\beta(t) \\ +9\max\{|v(t)|, |0.185w(t)|\} \end{pmatrix} dt. \tag{26}$$

Similarly, the energy model can be obtained for the Pioneer 3DX robot on the carpet floor.

To verify the correctness of the energy model in (26), the robot was allowed to move according to a designed velocity profile, as shown in Fig. 6(a). The modeling and experimental results of the battery current were then compared, as shown in Fig. 6(b). In the experiment, the robot accelerated to a desired velocity of 0.3 m/s within 3 s and then maintained this velocity. At 6 s, the angular velocity began to increase, reaching $\pi/2$ rad/s at 9 s. Finally, both the linear and angular velocities decreased at 10 s, reaching zero at 13 s. The identified parameters P_s and μ as given in (26) were used to calculate the modeling results.

In Fig. 6(b), the modeling results agree with the experimental data, which verified the correctness of the identified parameters.

B. Verifying Energy-Based Motion Planning

1) Simulations: To demonstrate the effectiveness of the proposed optimal motion planning for minimizing the energy consumption of a mobile robot, simulations on a two-wheeled mobile robot were performed on a flat road and on a macadam road. An optimal path was planned for the robot in an environment with wall-like obstacles. The environment contained 80 × 60 grids, and each grid had a square with 125-mm edges. The parameters used in the simulations were $r = 0.1$ m, $b = 0.2$ m, and $D_{\text{safe}} = 0.2$ m. The friction parameter μ on the flat road and on the macadam road was 0.05 and 0.08, respectively.

By using the developed A* path planner, the path was generated based on the proposed energy cost function (18), as shown in Fig. 7(a). Two other paths were also generated by using the A* path planner. Fig. 7(b) illustrates the generated path based on the shortest travel distance. In this case, the robot moved through a narrow space and might move relatively slowly for safety reasons. Fig. 7(c) illustrates the generated path that maintained a relatively large distance between the moving robot and surrounding obstacles. In this case, the robot must travel on the rough macadam floor, which causes the robot to consume more energy to enable it overcome high friction.

An optimal trajectory was then generated based on the path in Fig. 7(a). The robot was driven to pass across the selected waypoints with minimum energy consumption. Fig. 8 illustrates the trajectory along the waypoints generated by the proposed trajectory generation method. The energy consumption, travel time, and final velocity at each waypoint are listed in Table II. For comparison, trajectories with other criterion such as kinetic energy conservation [18], reduction of steering actuations [19], and trajectory smoothness [20] were also generated. The travel time, travel distance, and energy consumption achieved by using these approaches are given in Table III.

The aforementioned simulation results demonstrate the success of the proposed energy-saving motion planning for a wheeled mobile robot. The effects of load and flooring type on robot energy consumption were considered in path planning. By selecting the proper travel time and velocity at waypoints, the trajectory was further smoothed with minimum energy consumption.

2) Experiments: Further experiments were performed on a Pioneer 3DX mobile robot in an office environment. The Pioneer robot is a two-wheeled, differentially driven robot. The computer on the two-wheeled Pioneer 3DX is equipped with a Pentium III 800 MHz CPU and 256 MB of memory. The information on the local environment could be measured by using the ceiling camera in our laboratory [28], [29]. The control method reported in [30] and [31] was applied to control the robot and to track the planned trajectory in the experiments. The robot was localized by using a motor encoder. The sampling frequency of the control loop was set as 10 Hz. The current drawn from the batteries was measured by using the hardware in Fig. 3. The measurements were then transmitted to a desktop PC through a serial port line.

In the experiment, the robot was required to move toward its goal position. Obstacles such as boxes and robots were placed in the environment, as shown in Fig. 9. Floor types in the working environment include marble and carpet. The mass of the robot was 9 kg, and the friction constant f_v on the marble and carpet floors was approximately 0.3965 and 0.5877, respectively. Other parameters that were applied in the experiment were $V_{\max} =$

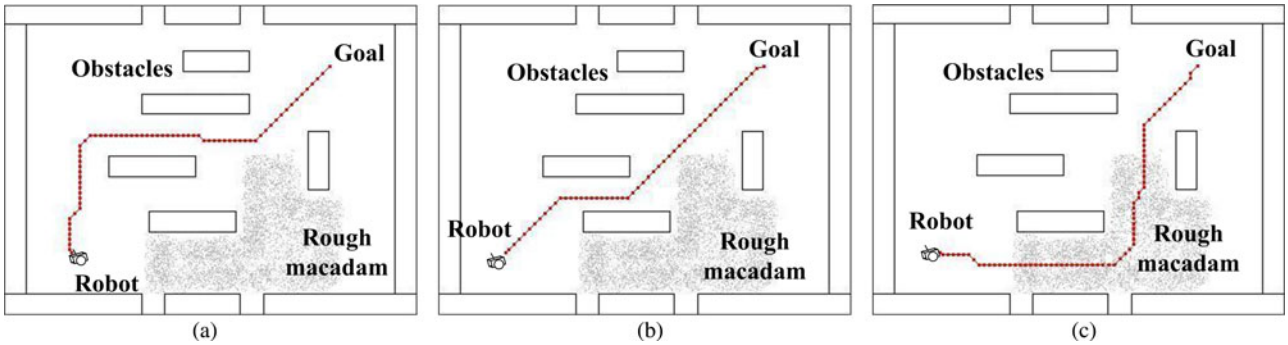

Fig. 7. Optimal path generation based on (a) minimum energy, (b) minimum travel distance, and (c) larger distance with obstacles.

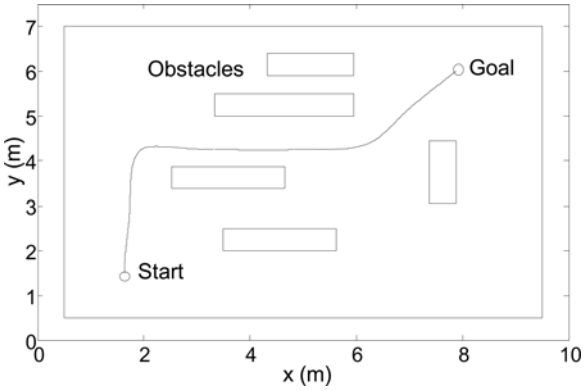

Fig. 8. Trajectory generation.

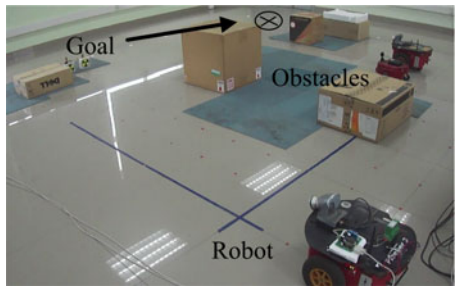

Fig. 9. Experiments in an office environment.

TABLE II
SIMULATION RESULTS OF TRAJECTORY OPTIMIZATION

Waypoint positions (m)	Energy consumption (J)	Travel time (s)	Velocity V_i (m/s)
(1.625, 1.500)	--	--	--
(1.700, 2.500)	94.17	5.68	0.2
(1.950, 4.250)	189.10	11.32	0.1
(3.325, 4.250)	294.40	17.72	0.35
(4.825, 4.250)	384.10	23.01	0.25
(6.200, 4.375)	490.31	28.93	0.2
(7.075, 5.250)	574.01	33.38	0.3
(7.875, 6.000)	683.59	40.32	0

TABLE III
SIMULATION RESULTS OF PERFORMANCE COMPARISON

	Travel time (s)	Travel distance (m)	Energy cost (J)
Proposed energy saving method	35.3	11.5	729.5
Kinetic energy saving method	39.2	10.1	808.5
Steering actuations reduction method	35.5	11.6	731.2
Trajectory smoothness method	36.5	14.5	788.2

0.7 m/s, $a_{\min} = -0.5$ m/s^2, $a_{\max} = 0.3$ m/s^2, $P_s = 17.8$ W, $r = 0.0925$ m, $m = 9$ kg, and $b = 0.2$ m.

The existing motion planning method [17] based on the Newton algorithm was first applied for energy optimization. This method assumed that the robot consumed less energy when moving along a shorter path. Fig. 10 illustrates that the robot moved along the shortest path on the carpet and passed the obstacles by using this method. When the robot moved near the obstacles, the robot had to move slowly to avoid collisions. The robot arrived at the goal position after approximately 15 s. The velocity profile along the shortest path is shown in Fig. 11(a). The current drawn from the batteries is shown in Fig. 11(b), where the dotted line represents the result calculated based on the energy model, and the solid line represents the actual current. The shortest path was not necessarily the minimum energy path because the load and the ground condition also affected the energy consumption significantly.

The proposed energy-saving motion planning method based on the energy model of Pioneer 3DX was then employed. A new path around the obstacles on the left-hand side was generated, as shown in Fig. 12. An optimal trajectory was further obtained along the waypoints selected from the generated path. Although the robot traveled a longer distance, it could move faster and took approximately 15 s to arrive at the goal position. The velocity profile along the trajectory is shown in Fig. 13(a), and the current drawn from the batteries is shown in Fig. 13(b).

The energy consumption of the robot in the aforementioned two methods is then compared. The energy consumption was calculated by integrating the current with time. Given that the travel times of the two methods were similar (approximately

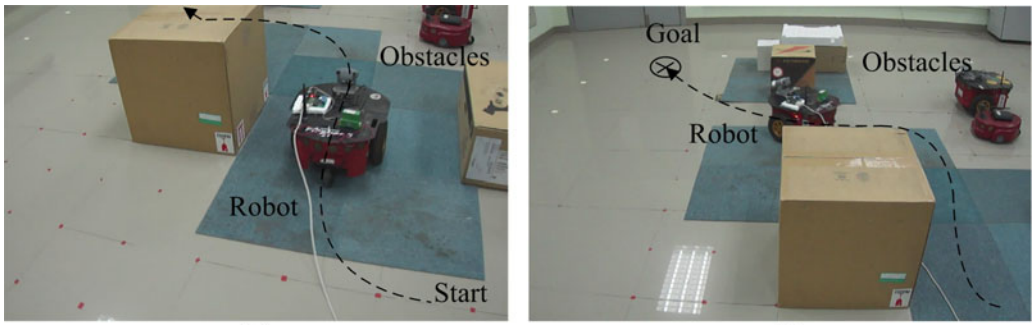

Fig. 10. Motion planning based on Newton algorithm for energy optimization.

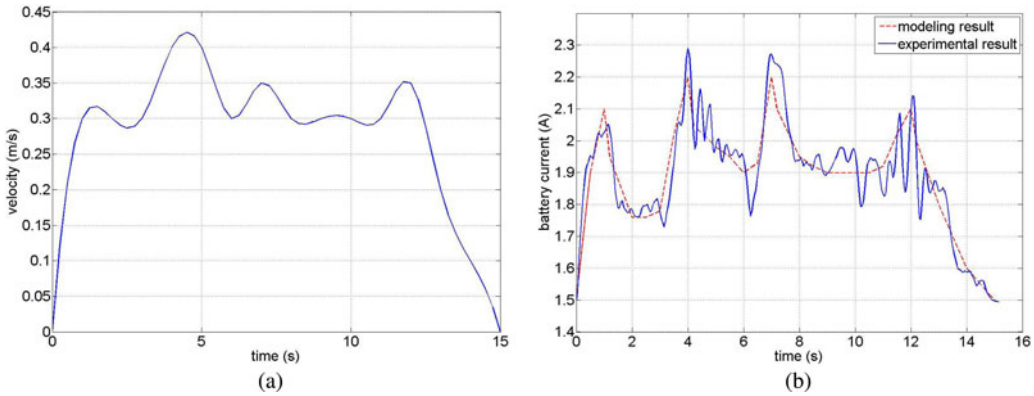

Fig. 11. Experimental results along the shortest path. (a) Velocity profile. (b) Current drawn from the batteries.

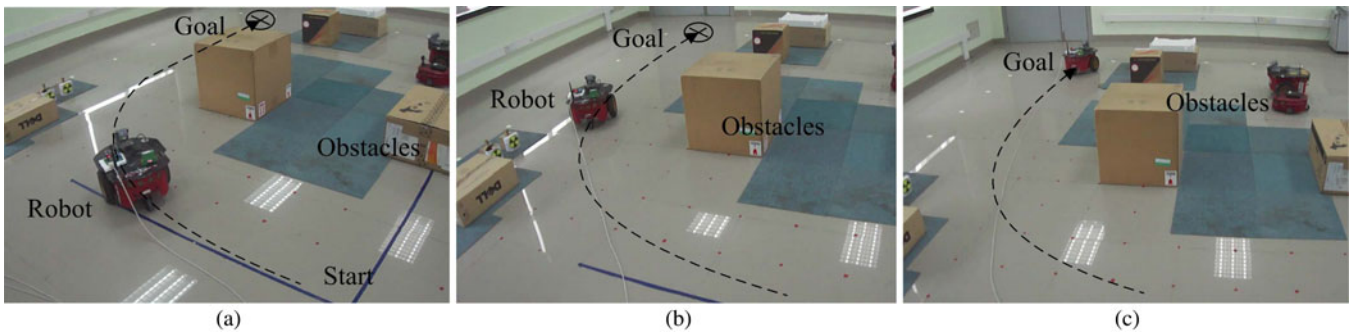

Fig. 12. Experiment using the energy-optimal motion planning: (a) 4, (b) 10, and (c) 15 s.

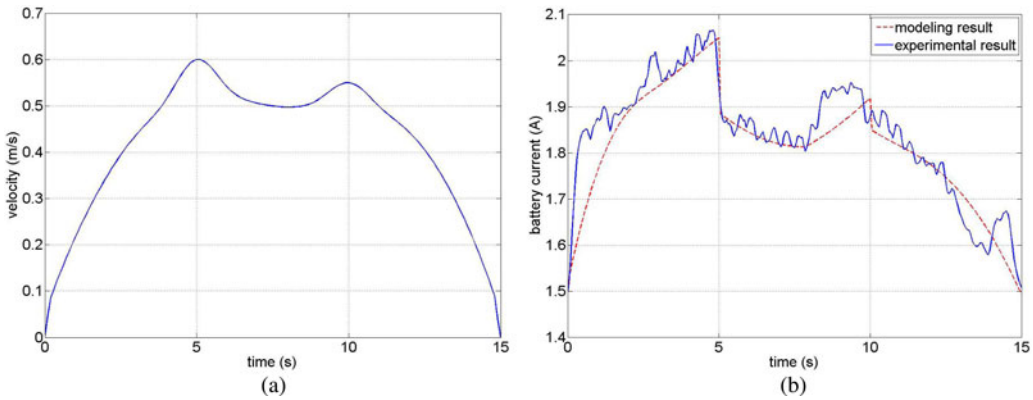

Fig. 13. Experimental results along the energy-saving trajectory. (a) Velocity profile. (b) Current drawn from the batteries.

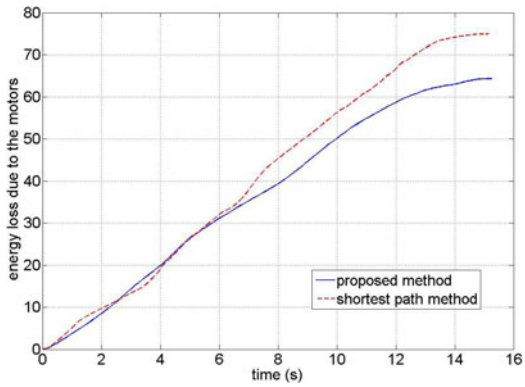

Fig. 14. Energy consumption of the motors with two methods.

TABLE IV
EXPERIMENT RESULTS

	Travel time(s)	Travel distance(m)	Energy cost(J)
Proposed energy saving method	15	6.53	330.8
Kinetic energy saving method	17.2	6.44	364.5
Steering actuations reduction method	15	6.60	334.2
Trajectory smoothness method	15.6	6.72	378.4

15 s), energy loss attributed to nonmechanical components E_{other} was almost the same (approximately 267 J). Thus, only energy consumption attributed to the motors are compared, as shown in Fig. 14. Energy consumption obtained by using the two methods was initially similar before different paths were selected. When the robot moved along the shortest path on the carpet, high friction resistance caused an increase in energy consumption, and our method was found to reduce energy consumption.

Experiments were conducted to demonstrate the effectiveness in terms of energy minimization of our trajectory generation method compared with some existing methods [18]–[20]. In these experiments, the waypoints that were generated by our proposed path planning method were used, but the trajectory smoothing methods along these waypoints varied. The travel time, travel distance, and energy consumption of the robot achieved by using these approaches is listed in Table IV. The method in [18] aimed to minimize energy by reducing the loss of kinetic energy, and the robot moved slowly with small variations in velocity. Longer travel time resulted in greater energy loss. The method in [19] could achieve minimum energy consumption by reducing steering actuations, which was similar to our method according to the energy model in (3). However, when using this method, the arrival time at each waypoint must be predesigned. The method in [20] used trajectory smoothness as the objective function in trajectory planning to save energy. This method did not consider other factors that affect energy consumption.

VI. CONCLUSION

To achieve minimum energy consumption, an optimal motion planning for a wheeled mobile robot is proposed in this paper, and an energy model of a two-wheeled mobile robot is then established. An A* path planner with new energy saving criterion in the cost function is utilized to generate an optimal path with minimum energy consumption. By utilizing the waypoints of the generated path, the trajectory is smoothed by using a parameterized cubic Bézier curve. The arrival time and velocity at each waypoint are optimized to minimize energy consumption in the trajectory generation. Experiments are performed to identify the modeling parameters for the Pioneer 3DX robot, and the effectiveness of the proposed approach in minimizing energy consumption is demonstrated in the simulations and in the experiments. Future studies will include an extension of the proposed motion planning methodology to multirobot applications for energy minimization. A proper energy management control [32] is also an important topic worthy of investigation.

REFERENCES

[1] S. E. Mushi, Z. Lin, and P. E. Allaire, "Design, construction, and modeling of a flexible rotor active magnetic bearing test rig," *IEEE/ASME Trans. Mechatronics*, vol. 17, no. 6, pp. 1170–1182, Dec. 2012.
[2] H. Kim and B. K. Kim, "Minimum-energy translational trajectory planning for battery-powered three-wheeled omni-directional mobile robots," in *Proc. IEEE Int. Conf. Control, Autom., Robot. Vis.*, 2008, pp. 1730–1735.
[3] Y. Mei, Y. Lu, C. Lee, and Y. Hu, "Energy-efficient mobile robot exploration," in *Proc. IEEE Int. Conf. Robot. Autom.*, 2006, pp. 505–511.
[4] Y. Wang, C. Chen, and C. Sung, "System design of a weighted-pendulum-type electromagnetic generator for harvesting energy from a rotating wheel," *IEEE/ASME Trans. Mechatronics*, vol. 18, no. 2, pp. 754–763, Apr. 2013.
[5] A. Jafari, N. G. Tsagarakis, and D. G. Caldwell, "A novel intrinsically energy efficient actuator with adjustable stiffness (AwAs)," *IEEE/ASME Trans. Mechatronics*, vol. 18, no. 1, pp. 355–365, Feb. 2013.
[6] R. Katoh, O. Ichiyama, T. Yamamoto, and F. Ohkawa, "A realtime path planning of space manipulator saving consumed energy," in *Proc. IEEE Int. Conf. Ind. Electron., Control Instrum.*, 1994, pp. 1064–1067.
[7] K. Wakita, J. Huang, P. Di, K. Sekiyama, and T. Fukuda, "Human-walking-intention-based motion control of an omnidirectional-type cane robot," *IEEE/ASME Trans. Mechatronics*, vol. 18, no. 1, pp. 285–296, Feb. 2013.
[8] J. Biesiadecki, P. C. Leger, and M. Maimone, "Tradeoffs between directed and autonomous driving on the mars exploration rovers," *Int. J. Robot. Res.*, vol. 26, no. 1, pp. 91–104, 2007.
[9] K. Tu, "Design of fuzzy potential energy (FPE) for control of a soccer robot," in *Proc. IEEE Int. Conf. Netw. Sens. Control*, 2004, vol. 2, pp. 1105–1109.
[10] Y. Wu, D. Sun, W. Huang, and N. Xi, "Dynamics analysis and motion planning for automated cell transportation with optical tweezers," *IEEE/ASME Trans. Mechatronics*, vol. 18, no. 2, pp. 706–713, Apr. 2013.
[11] T. Howard and A. Kelly, "Optimal rough terrain trajectory generation for wheeled mobile robots," *Int. J. Robot. Res.*, vol. 26, pp. 141–166, 2007.
[12] G. Zhang, G. K. Fricke, and D. P. Garg, "Spill detection and perimeter surveillance via distributed swarming agents," *IEEE/ASME Trans. Mechatronics*, vol. 18, no. 1, pp. 121–129, Feb. 2013.
[13] H. Chitsaz, S. LaValle, D. Balkcom, and M. Mason, "Minimum wheel-rotation paths for differential-drive mobile robots," *Int. J. Robot. Res.*, vol. 28, no. 1, pp. 66–80, 2009.
[14] Y. Mei, Y. Lu, Y. Hu, and C. Lee, "Deployment of mobile robots with energy and timing constraints," *IEEE Trans. Robot.*, vol. 22, no. 3, pp. 507–522, 2006.
[15] T. Wang, B. Wang, H. Wei, Y. Cao, M. Wang, and Z. Shao, "Staying-alive and energy-efficient path planning for mobile robots," in *Proc. Amer. Control Conf.*, 2008, pp. 868–873.

[16] J. Chen, J. Li, S. He, Y. Sun, and H. Chen, "Energy-efficient coverage based on probabilistic sensing model in wireless sensor networks," *IEEE Commun. Lett.*, vol. 14, no. 9, pp. 833–835, Sep. 2010.
[17] I. Duleba and J. Z. Sasiadek, "Nonholonomic motion planning based on Newton algorithm with energy optimization," *IEEE Trans. Control Syst. Technol.*, vol. 11, no. 3, pp. 355–363, May 2003.
[18] A. Barili, M. Ceresa, and C. Parisi, "Energy-saving motion control for an autonomous mobile robot," in *Proc. IEEE Int. Symp. Ind. Electron.*, 1995, vol. 2, pp. 674–676.
[19] J. Yang, Z. Qu, J. Wang, and K. Conrad, "Comparison of optimal solutions to real-time path planning for a mobile vehicle," *IEEE Trans. Syst., Man, Cybern. A, Syst. Humans*, vol. 40, no. 4, pp. 721–731, Jul. 2010.
[20] A. M. Hussein and A. Elnagar, "On smooth and safe trajectory planning in 2D environments," in *Proc. IEEE Int. Conf. Robot. Autom.*, 1997, vol. 4, pp. 3118–3123.
[21] Y. Mei, Y. Lu, Y. Hu, and C. Lee, "Energy-efficient motion planning for mobile robots," in *Proc. IEEE Int. Conf. Robot. Autom.*, vol. 5, New Orleans, 2004, pp. 4344–4349.
[22] P. E. Hart, N. J. Nilsson, and B. Raphael, "A formal basis for the heuristic determination of minimum cost paths," *SIGART Newslett.*, vol. 37, pp. 28–29, 1972.
[23] D. Wang and C. Low, "Modeling and analysis of skidding and slipping in wheeled mobile robots: control design perspective," *IEEE Trans. Robot.*, vol. 24, no. 3, pp. 676–687, Jun. 2008.
[24] F. Gerald, *Curves and Surfaces for Computer-Aided Geometric Design*, 4th ed. New York, NY, USA: Elsevier, 1997.
[25] S. Liu, D. Sun, C. Zhu, and W. Shang, "A dynamic priority strategy in decentralized motion planning for formation forming of multiple mobile robots," in *Proc. IEEE/RSJ Int. Conf. Int. Robots Syst.*, 2009, pp. 3774–3779.
[26] B. Lau, C. Sprunk, and W. Burgard, "Kinodynamic motion planning for mobile robots using splines," in *Proc. IEEE/RSJ Int. Conf. Int. Robot. Syst.*, 2009, pp. 2427–2433.
[27] *Pioneer 3 Operations Manual, ver. 5*, Active media Robotics, Amherst, NH, 2007.
[28] H. Chen, D. Sun, J. Yang, and J. Chen, "SLAM based global localization for multi-robot formations in indoor environment," *IEEE/ASME Trans. Mechatronics*, vol. 15, no. 4, pp. 561–574, Aug. 2010.
[29] S. Liu, D. Sun, and C. Zhu, "Coordinated motion planning for multiple mobile robots along designed paths with formation requirement," *IEEE/ASME Trans. Mechatronics*, vol. 16, no. 6, pp. 1021–1031, Dec. 2011.
[30] Z. P. Jiang and H. Nijmeijer, "Tracking control of mobile robots: a case study in backstepping," *Automatica*, vol. 33, no. 7, pp. 1393–1399, 1997.
[31] J. Chen, D. Sun, J. Yang, and H. Chen, "A leader-follower formation control of multiple nonholonomic mobile robots incorporating receding-horizon scheme," *Int. J. Robot. Res.*, vol. 29, no. 6, pp. 727–747, 2010.
[32] B. Geng, J. K. Mills, and D. Sun, "Energy management control of microturbine-powered plug-in hybrid electric vehicles using the telemetry equivalent consumption minimization strategy," *IEEE Trans. Veh. Technol.*, vol. 60, no. 9, pp. 4238–4248, Nov. 2011.

Shuang Liu received the B.Sc. degree from the Department of Precision Machinery and Instrumentation, University of Science and Technology of China, Hefei, China, in 2005, and the Ph.D. degree from the Joint Research Center of the City University of Hong Kong, Kowloon, Hong Kong, and the University of Science and Technology of China, Suzhou, China, in 2010.

Since 2010, he has been a Postdoctoral Fellow in the Department of Mechanical and Biomedical Engineering, City University of Hong Kong. His research interests include mobile robots, multirobot systems, and motion planning.

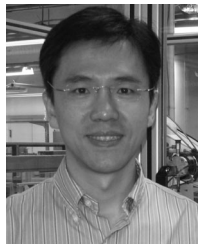

Dong Sun (S'95–A'97–M'00–SM'08) received the B.Sc. degree in mechatronics and the M.Sc. degree in biomedical engineering from Tsinghua University, Beijing, China, and the Ph.D. degree in robotics and automation from the Chinese University of Hong Kong, Hong Kong.

He was a Postdoctoral Researcher at the University of Toronto, Toronto, ON, Canada, and a Research and Development Engineer in Ontario industry. Since 2000, he has been with the City University of Hong Kong, Kowloon, Hong Kong, where he is currently a Professor in the Department of Mechanical and Biomedical Engineering. His research interests include robotics manipulation, multirobot systems, motion control, and cell-based bioengineering.

Dr. Sun was an Associate Editor for the IEEE TRANSACTIONS ON ROBOTICS from 2004 to 2008. He currently serves as a Technical Editor for the IEEE/ASME TRANSACTIONS ON MECHATRONICS.